The Kinetics of Ligand Binding by an Adenine-Sensing Riboswitch

J. Kenneth Wickiser,[‡,§] Ming T. Cheah,[||] Ronald R. Breaker,*[,‡,||] and Donald M. Crothers*[,‡,⊥]

Departments of Molecular Biophysics and Biochemistry, Molecular, Cellular and Developmental Biology, and Chemistry, Yale University, New Haven, Connecticut 06520-8103

Received May 27, 2005; Revised Manuscript Received July 19, 2005

ABSTRACT: A riboswitch within the 5′ untranslated region (UTR) of the *Bacillus subtilis pbuE* mRNA binds adenine and related analogues in the absence of protein factors; excess adenine added to bacterial growth media triggers activation of a reporter gene that carries this riboswitch. To assess whether the riboswitch reaches thermodynamic equilibrium, or is operated by the kinetics of ligand binding and RNA transcription, we examined the detailed equilibrium and kinetic parameters for the complex formation between the aptamer domain of this riboswitch and the ligands adenine, 2-aminopurine (2AP), and 2,6-diaminopurine (DAP). Using a fluorescence-based assay, we have confirmed that adenine and 2AP have nearly equal binding affinity, with K_D values for 2AP ranging from 250 nM to 3 μM at temperatures ranging from 15 to 35 °C, while DAP binds with much higher affinity. The association rate constant, however, favors adenine over DAP and 2AP by 3- and 10-fold, respectively, at 25 °C. Furthermore, the rate constants for adenine association and dissociation with the aptamer suggest that the *pbuE* riboswitch could be either kinetically or thermodynamically controlled depending upon the time scale of transcription and external variables such as temperature. We cite data that suggest kinetic control under certain conditions and illustrate with a model calculation how the system can switch between kinetic and equilibrium control. These findings further support the hypothesis that many riboswitches rely on the kinetics of ligand binding and the speed of RNA transcription, rather than simple ligand affinity, to establish the concentration of metabolite needed to trigger riboswitch function.

Riboswitches are untranslated mRNA elements that directly bind ligands and alter the expression of genes that are almost always associated with biosynthesis or transport of the target ligand or a closely related compound. Riboswitches have been demonstrated to function as essential control elements for the metabolism of guanine, adenine, flavin mononucleotide (FMN), coenzyme B_{12}, thiamin pyrophosphate (TPP), *S*-adenosylmethionine (SAM), glucosamine 6-phosphate (GlcN6P), lysine, and glycine (*1*−*6*). Riboswitches are generally comprised of two modular domains of contiguous RNA sequence: the apatamer, or ligand binding domain, and the expression platform, the structural domain which senses the ligand occupancy status of the aptamer domain and modulates the expression of the downstream gene set. These RNA-based genetic control elements have been shown to directly modulate transcription termination and translation initiation (*7*, *8*). Furthermore, evidence is mounting that riboswitches can directly control mRNA splicing (*9*, *10*) and stability (*6*).

In a recent study, the mechanism of the FMN-sensitive riboswitch that controls the *ribD* gene of *Bacillus subtilis* was characterized. The function of this riboswitch was found to depend on the time scale of transcription as the RNA polymerase transcribes the expression platform and is also affected by the kinetics of ligand binding to the riboswitch (*11*). A hallmark of a kinetically operated riboswitch is that equilibrium between the RNA aptamer and its ligand is not achieved by the time the genetic decision must be made, and therefore the individual rate constants for ligand association and dissociation are more important for describing the system than is the equilibrium dissociation constant (K_D). Thus, the *ribD* riboswitch appears to be a kinetically rather than a thermodynamically controlled sensor of cellular FMN concentration.

The kinetic nature of the FMN riboswitch resolved a discrepancy in the values for ligand concentrations needed to trigger riboswitch-mediated transcription termination in vitro versus the K_D values for ligand−RNA complex formation measured under similar assay conditions (*12*). In general, the ligand concentration (B_{50}) that results in 50% occupancy of the aptamer binding sites at the time the genetic decision is made differs from K_D for several classes of riboswitch aptamers, implying that the binding process is not at equilibrium. Therefore, our observations with the FMN riboswitch also led us to speculate that many other riboswitches employing transcriptional termination might likewise be kinetically controlled. In this report we sought to dissect the mechanism of the *pbuE* riboswitch (formerly named *ydhL*), which controls transcriptional termination of

* To whom correspondence should be addressed. R.R.B.: phone, (203) 432-9389; fax, (203) 432-6604; e-mail, ronald.breaker@yale.edu. D.M.C.: phone, (203) 432-5204; fax, (203) 432-6144; e-mail, donald.crothers@yale.edu.

[‡] Department of Molecular Biophysics and Biochemistry, Yale University.

[§] Current address: Rockefeller University, 1230 York Ave., Box 226, New York, NY 10021.

[||] Department of Molecular, Cellular and Developmental Biology, Yale University.

[⊥] Department of Chemistry, Yale University.

10.1021/bi051008u CCC: $30.25
Published on Web 09/13/2005

a gene whose product is involved in adenine transport (*13*, *14*).

Adenine riboswitches were recognized as a subset of conserved RNA elements whose members were found to bind guanine (*15*). Subset representatives each carried a single C to U mutation in the conserved core of the aptamer that has since been shown to form a G-C base pair in guanine-specific aptamers and to form an A-U base pair in adenine-specific aptamers (*16*−*20*). Furthermore, this adenine riboswitch is the first example of a genetic ON switch, or a riboswitch that upregulates gene expression when docked with the target metabolite. In vivo experiments support the assertion that the PbuE protein rids the cell of excess adenine and hypothanthine (*14*), leading the investigators to propose that this efflux pump may function to protect the cell against a buildup of purine base analogues to toxic levels. In this study, we examined the stability of the aptamer domain of the *pbuE* riboswitch and determined the thermodynamic and kinetic properties of adenine, 2AP, and DAP ligand binding (Figure 1A).

MATERIALS AND METHODS

RNA Preparation. RNA constructs were prepared as previously described (*11*).

Riboswitch Ligands. Adenine, 2AP, and DAP were obtained from Sigma, suspended in deionized H_2O at a concentration of 10 mM, and stored protected from light at −20 °C. A minimum of HCl was added to solubilize a concentrated stock solution of adenine in H_2O. Concentrations of the compounds were measured optically using the extinction coefficients reported by the supplier.

Fluorescence-Based K_D Determinations. 2AP was held constant at 50 nM, and its fluorescence was measured while titrating in RNA. The samples were suspended in reaction buffer (RB) containing 50 mM Na-MOPS[1] (pH 7.5 at 25 °C), 100 mM KCl, and 2 mM $MgCl_2$, and the RNA−2AP samples were kept on ice prior to use. Before measurements were taken, air was removed from the samples using helium gas, and the samples were transferred to a quartz cuvette, degassed with helium again, and placed in the multicell peltier block of a Cary Eclipse fluorometer and held at 15 °C. We utilized a program written by Dr. Mark Fisher of Varian Inc. to perform emission scans at 15, 20, 25, 30, and 35 °C while waiting 7 min between each temperature change to allow for reequilibration of the 2AP−RNA complex. Slit widths and PMT voltage were set for maximum emission. The ligands were not photodegraded during the course of the measurements, as judged by recovery of the original fluorescence signal under the starting conditions.

Ligand Binding Kinetics. Experiments were conducted as described previously (*11*). The fluorescence signal was generated by exciting at 305 nm (2AP) using 0.5 mm slit widths and monitored using a 350 nm long pass colored glass filter from Oriel. All stopped-flow experiments were carried out in RB.

Association Rate Constants. The k_{on} values were determined by mixing RNA (in excess over 2AP) held constant at 50 nM in RB at 20, 25, 30, and 37 °C in an Applied Photophysics stopped-flow spectrometer in fluorescence mode. Transients faster than 1 ms are not resolved by this instrument. The time constants derived from the data generated with each sample were averaged, inverted, and then plotted against the final RNA concentration to obtain second-order rate constants from the slope of this plot. The mean of the measured rate constants at each temperature was incorporated into an Eyring plot to determine the activation enthalpy barrier magnitude by plotting $\ln(k/T)$ versus $1/T$ from the equations (*21*):

$$\ln\left(\frac{k}{T}\right) = -\frac{\Delta H^{\ddagger}}{R}\frac{1}{T} + \ln\left(\frac{k_B}{h}\right) + \frac{\Delta S^{\ddagger}}{R}$$

$$\Delta G^{\ddagger} = -RT\ln\left(\frac{kh}{k_B T}\right)$$

For the experiments in which 2AP was in excess over RNA, the data also fit a first-order exponential response. All curve fitting was conducted using Microcal Origin and Microsoft Excel.

Dissociation Rate Constants. The k_{off} value for 2AP was established using the stopped-flow device and a modified dilution−relaxation method. The RNA−2AP complex in RB was diluted with an equivalent amount of buffer and varying concentrations of adenine. The fluorescence signal increase due to the dissociation of the 2AP−RNA complex was monitored over time. At high concentrations of adenine, the fluorescence signal fit a single-order exponential response, from which a time constant of 2AP dissociation was generated. The same data were used to attain the k_{on} and k_{off} for adenine using known concentrations of all components of the reaction and the rate constants for 2AP by modeling the reaction with the program Berkeley Madonna (version 8.1β11, http://www.berkeleymadonna.com). A simple two-state binding model was used wherein 2AP and adenine compete for the aptamer RNA. To measure the kinetic parameters for DAP binding, a similar kinetic competition experiment between 2AP and DAP was conducted, and the data were then modeled as described above.

Thermal Denaturation Experiments. Denaturation assays monitoring fluorescence were conducted in a Cary Eclipse fluorometer using an excitation wavelength of 310 nm and monitoring emission at 370 nm for 2AP (300 and 345 nm for DAP). Slit widths and PMT voltage were adjusted to optimize the signal at 15 °C. The temperature was changed at a rate no faster than 1 °C/min. Dry nitrogen was delivered to avoid condensation on the cuvettes. Each cuvette contained at least 300 μL of solution covered with 400 μL of mineral oil to avoid evaporation. Denaturation experiments monitoring optical absorption were conducted using a Cary 1 UV−vis spectrophotometer in double-beam mode. Absorbance was measured at 260 nm. A slit width of 1 nm and an averaging time of 3 s were used. Other details were as described for experiments monitoring fluorescence.

In silico Structural Energetics Prediction. The program RNAstructure (*22*) was used with default settings to predict the energetics and equilibrium structures at 37 °C of the nascent RNA as described in Figure 7. The free energy of 70 *pbuE* served as the base value to determine the stability parameter ($\Delta\Delta G$) for each step of the nascent transcript.

[1] Abbreviations: NTP, nucleoside triphosphate; EDTA, ethylenediaminetetraacetic acid; PMT, photomultiplier tube; MOPS, morpholinopropanesulfonic acid; UV, ultraviolet; PCR, polymerase chain reaction; RNAP, RNA polymerase.

In-Line Probing Assay. The 175 *pbuE* RNA was prepared and assayed using an in-line probing analysis as reported previously (*23*). DNA primers used to PCR amplify the appropriate template for transcription by T7 RNA polymerase were synthesized by the HHMI Keck Biotechnology Resource Laboratory at Yale University and used without purification.

RESULTS AND DISCUSSION

Binding Equilibria of an Adenine Aptamer. Previously (*20*), a biochemical method termed in-line probing was used to determined equilibrium dissociation constants for the *pbuE* riboswitch aptamer of ~300 nM for adenine and 2AP. In the current study, we exploited the intrinsic fluorescence of 2AP to extract equilibrium and dynamic properties for the binding of this compound and for adenine (nonfluorescent) and DAP (weakly fluorescent) (*24*). Specifically, we took advantage of substantial fluorescence quenching that occurs upon 2AP binding by the 70-nucleotide version of the *pbuE* aptamer (termed 70 *pbuE*) (Figure 1B, inset), utilizing as well the fluorescence change that occurs when 2AP is replaced by adenine or DAP.

Bacteria survive over a range of temperatures, which entails considerable variation in equilibrium and kinetic constants for ligand binding. We therefore determined the K_D values for the RNA−2AP complex at several temperatures, using the data to calculate the corresponding enthalpy of the binding reaction (Figure 1B,C). Despite the difference in buffer conditions, the apparent K_D of 764 nM at 25 °C is consistent to within 2.5-fold of the previous estimates of 300 nM for the K_D of 2AP and the *pbuE* aptamer derived from in-line probing assays (*20*). Additionally, the data are consistent with a 1:1 stoichiometry between RNA and 2AP (Figure 1B). As an exothermic reaction, the binding event is less efficient at higher temperatures. The K_D rises from 250 to 3000 nM, and the corresponding value of $\Delta G°$ decreases from −8.7 to −7.8 kcal/mol as the temperature is increased from 15 to 35 °C (Figure 1C, inset). The K_D value of the *pbuE* aptamer for 2AP is over an order of magnitude larger (weaker binding) than that measured for the *ribD* aptamer for its corresponding FMN ligand at 15 °C and over 2 orders of magnitude larger at 35 °C (*11*).

Analysis of the temperature dependence using the van't Hoff equation yielded −21.8 kcal/mol (Figure 1C) for the heat of interaction between the ligand and RNA, which is over three times greater than that for the FMN-sensitive aptamer and its ligand (−6.02 kcal/mol) (*11*). The enthalpy of binding is likely to involve increased base stacking associated with a ligand-dependent rearrangment of secondary and tertiary RNA structure, as well as physical contact between the ligand and the RNA. One possible explanation for the large value of binding enthalpy is that *pbuE* has a higher number of nucleotides that change structure upon binding its target ligand compared to the FMN binding *ribD* riboswitch. However, major secondary structural rearrangment was not observed by previous analysis using the in-line probing assay (*20*), which showed remarkably little change in the structure of the phosphodiester backbone of the adenine aptamer upon the addition of a saturating concentration of ligand. Resolution of the conformational change upon binding awaits detailed structural studies.

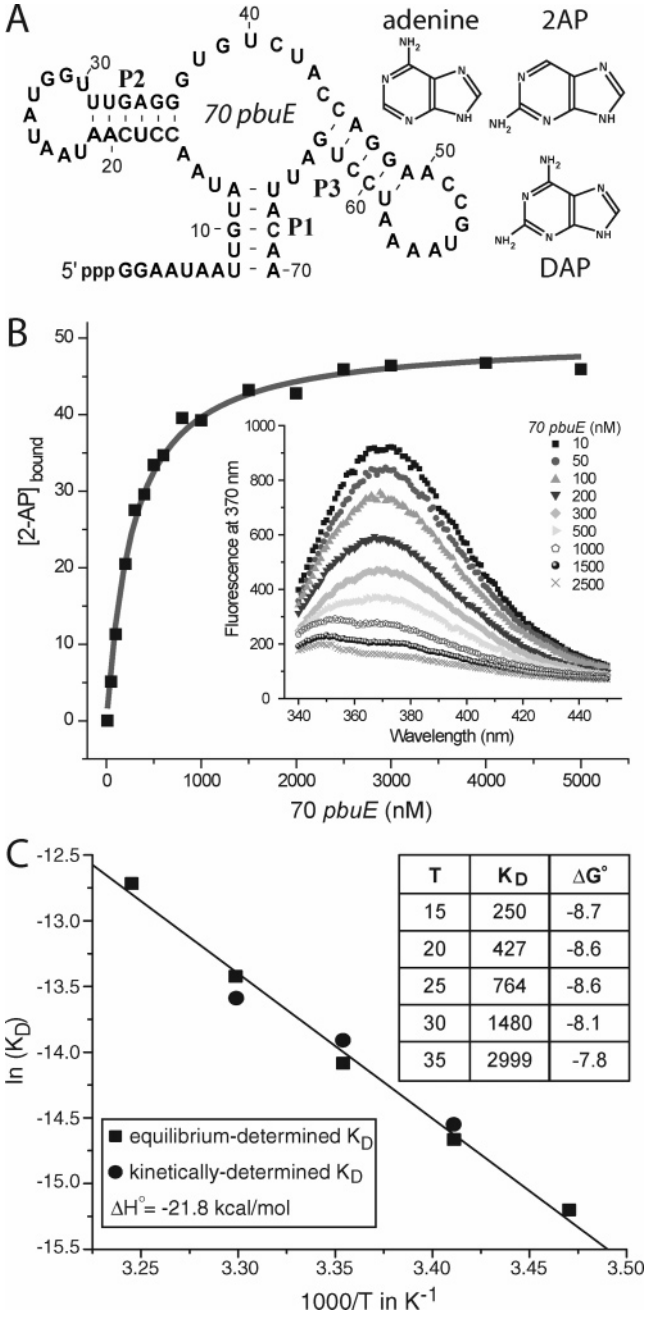

T	K_D	$\Delta G°$
15	250	-8.7
20	427	-8.6
25	764	-8.6
30	1480	-8.1
35	2999	-7.8

FIGURE 1: Fluorescence binding assays with 2AP and 70 *pbuE*. (A) Sequence and secondary structure model for 70 *pbuE* RNA and the structures of adenine, 2-aminopurine (2AP), and 2,6-diaminopurine (DAP). (B) Concentration of bound 2AP in nanomolar versus concentration of 70 *pbuE* as determined by 2AP fluorescence quenching and fit to a standard quadratic solution to the equation for K_D given 1:1 stoichiometry. Inset: emission wavelength scans for samples in the dilution series of RNA in 50 nM 2AP at 15 °C. (C) van't Hoff plot of 70 *pbuE* and 2AP by fluorescence using the equilibrium-derived K_D values (squares) and the kinetically determined K_D values (circles; see Figures 3 and 4 for additional details). The slope indicates an enthalpy value of $\Delta H° = -21.8$ kcal/mol. The inset is a table of K_D values in nanomolar and $\Delta G°$ in kilocalories per mole calculated by $\Delta G° = -RT \ln(K_D)$.

For maximum responsiveness, a thermodynamically controlled riboswitch, or one that achieves equilibrium between aptamer and ligand, might be expected to exhibit a K_D value that is nearly equivalent to the mean cellular concentration of the metabolite. A natural cellular concentration of adenine recently reported to be approximately 30 μM (*14*) (at 37 °C)

is considerably larger than the K_D value of about 3.4 μM at 37 °C estimated from the data in Figure 1C. It is characteristic of kinetically controlled riboswitches that the cellular concentration is larger than the K_D value, so we conclude that the switch is likely to be kinetically controlled under these conditions. However, since the K_D and estimated cellular concentrations differ by less than an order of magnitude, this conclusion remains tentative.

Given that the riboswitch binds other physiologically relevant adenine analogues (*20*), if the riboswitch operates at equilibrium for each ligand and if adenine is the true metabolic ligand, the normal concentration of tight-binding analogues such as DAP must be far below the concentration of adenine required for activation, to avoid accidentally tripping the genetic switch. It is possible that the switch operates at equilibrium for some ligands and is kinetically controlled for others. Furthermore, a change of temperature could cause a shift in the mode of control. We report below model calculations that show how the equilibrium and kinetic variables interact with transcription rate to vary the control mechanism.

Aptamer Secondary Structural and Binding Equilibria. To investigate the relationship between ligand affinity and the temperature-dependent structure of the aptamer, thermal denaturation assays were performed on aptamer RNAs having wild-type and mutated P1 stems (Figures 1A and 2A). The P1 helix, which is comprised of the distal-most regions of the primary sequence (nucleotides 8−12:70−66), is essential for ligand binding. Furthermore, interpretation of the purine aptamer phylogeny implies the existence of a sequence-nonspecific P1 stem (*15*). Thermal denaturation experiments monitor the heat-induced unfolding of RNA structural domains by observing the absorbance changes as a function of temperature. In the presence of adenine, the aptamer mutants with strengthened (70S *pbuE*) and weakened (70W pbuE) P1 structures have respectively higher and lower melting temperature (T_m) values of the main structural transition as determined by absorbance-monitoring thermal denaturation assays (Figure 2B and Table 1). Additional denaturation experiments showed that the UV-determined structural transition is not affected within the accuracy of the measurement by increasing the RNA concentration to 5 μM nor by the presence of up to 20 μM adenine or 5 μM 2AP or DAP (data not shown). The breadth of the transition for the 70S *pbuE* RNA from fully bound to unbound is narrower compared to the wild-type or 70W *pbuE* RNA (Figure 2C) as determined by monitoring the fluorescence during the thermal denaturation of a complex of the 70 *pbuE* aptamer RNA and DAP. However, the major T_m value determined from the derivative fluorescence melting profiles is little affected by the mutations. As seen in Table 1, the major fluorescence-determined T_m values lie below the main UV-determined structural transitions but above the estimated T_m values for shoulders on the derivative curves. The combined heats of ligand dissociation and melting of critical parts of the aptamer domain yield a maximum in the fluorescence denaturation profile that cannot be associated with a melting transition that is visible in the UV, which monitors the entire RNA. These data indicate that the ligand is released prior to the denaturation of the major structural elements of the aptamer, implying that the destruction of essential tertiary structural elements and delicate secondary structural elements is responsible for the release of the ligand.

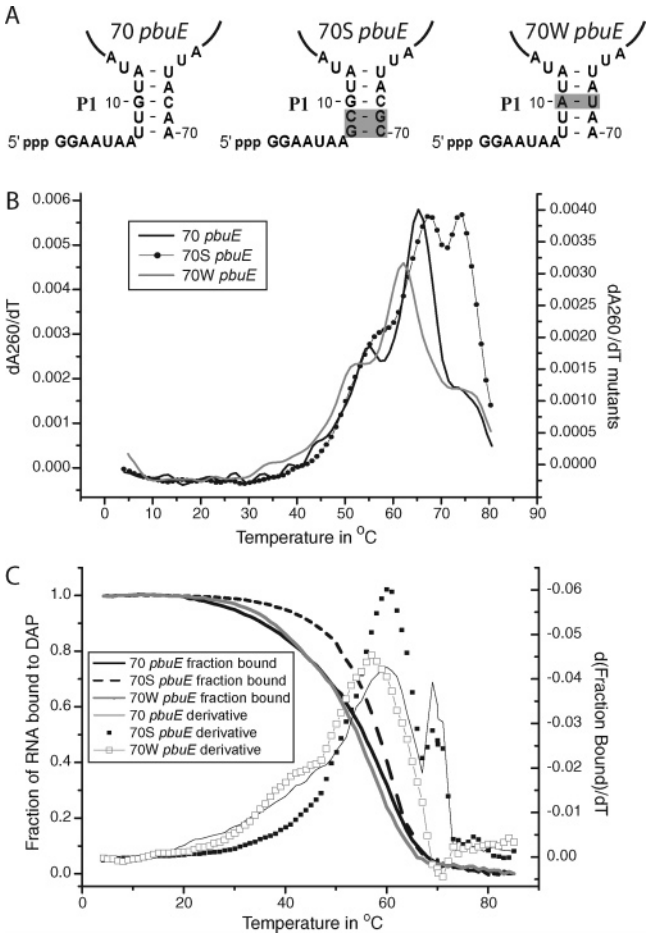

FIGURE 2: Stability of stem 1. (A) Diagram of the wild-type P1 stem and mutations. The highlighted bases indicate P1 stem mutations where 70S and 70W are the strengthened and weakened versions of 70 *pbuE*, respectively. (B) Differential absorbance at 260 nM of RNAs subject to thermal denaturation. The black line represents 500 nM 70 *pbuE* RNA and 20 μM adenine. The closed circles and gray line represent the 70S *pbuE* and 70W *pbuE* constructs at similar concentrations of RNA and adenine. (C) Fraction of RNA complexed and derivative of fraction complexed as determined by the fluorescence quenching of DAP for 70 *pbuE*, 70S *pbuE*, and 70W *pbuE* at 5 μM each of the RNA and adenine.

Table 1: T_m Values from UV and Fluorescence Derivative Melting Curves

RNA	UV T_m values[a] (°C)	fluorescence T_m values[b] (°C)
70 *pbuE*	(55),[c] 65	60
70S *pbuE*	(57), 67, 74	59
70W *pbuE*	(52), 62	(42), 57

[a] Measured with 0.5 μM RNA and 20 μM adenine. [b] Measured with 5.0 μM RNA and 5.0 μM DAP. [c] Values in parentheses are estimated T_m values for shoulders in the derivative melting curves.

Kinetics of Ligand Binding to an Adenine Aptamer. From our previous analysis of a FMN-responsive riboswitch within *B. subtilis*, it was concluded that kinetic parameters such as the association rate constant and the RNA−ligand complex lifetime were more important than K_D in describing the behavior of the system because that riboswitch was driven kinetically, rather than thermodynamically (*11*). To investigate whether riboswitches that use ligand-activated tran-

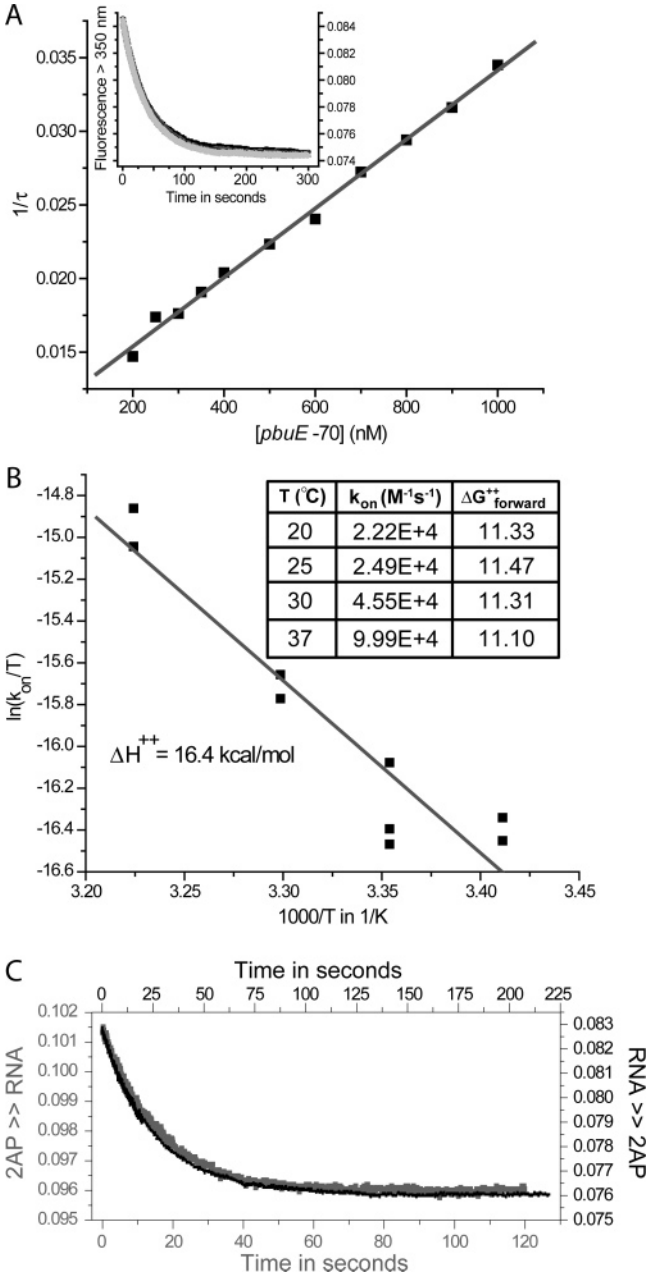

FIGURE 3: Association rate constant of 2AP and 70 *pbuE* from stopped-flow fluorescence of 2AP. (A) Inverted time constant of the association reaction versus final RNA concentration with 50 nM 2AP (final), the slope of which yields the k_{on}. The inset is a sample of several stopped-flow fluorescence quenching data sets for 25 °C, 50 nM 2AP (final), and 1000 nM 70 *pbuE* (final). (B) Eyring plot of the association rate constant using 50 nM 2AP and 70 *pbuE* RNA. Each black square represents a k_{on} value generated from data similar to panel A. The inset is a table of association rate constants and the associated activation free energies in kilocalories per mole computed by Eyring theory assuming a transmission coefficient of unity (see Materials and Methods section for the equation). (C) The binding event is a two-state process. Sample data sets for (black) ligand association using RNA in excess over 2AP (50 nM 2AP and 1200 nM 70 pbuE at 25 °C) and (gray) ligand association using 2AP in excess over RNA (500 nM 2AP and 100 nM 70 *pbuE* at 25 °C). Both data sets fit a single exponential response, suggesting the binding event is a two-state process.

scriptional antitermination might act as kinetically controlled switches, the kinetics of ligand binding to 70 *pbuE* were investigated (Figure 3). The association rate constant for 2AP, studied using a stopped-flow fluorometer and pseudo-first-order conditions of RNA in excess over ligand (Figure 3A), was determined to be on the order of 10^4 M^{-1} s^{-1} (Figure 3B, inset). This value is about an order of magnitude smaller (slower) than the k_{on} of the aptamer domain of the FMN-sensitive riboswitch and its target ligand (*11*). Assuming 1 μM 2AP, in excess over RNA, the time constant (the time required for e^{-1} of a reaction to occur) for the binding reaction ranges from 45 s at 20 °C to 10 s at 35 °C. Given a 10-fold increase in ligand concentration, a corresponding 10-fold reduction in the time constant for the binding reaction should occur. In addition, analysis using an Eyring plot determined that the activation enthalpy barrier (*25*) of the forward binding reaction of 2AP to 70 *pbuE* was 16.4 kcal/mol, which is approximately equal to that of FMN−*ribD* riboswitch binding (Figure 3B).

Finally, to investigate whether the forward binding reaction of 2AP was truly a single step, the association rate constant measurements were repeated under conditions of ligand in excess over RNA (Figure 3C). The binding kinetics followed a first-order exponential decay, supporting a two-state binding process with no detectable intermediates or evidence of an appreciable population of misfolded RNAs with the caveat that the stopped flow instrument used has a dead time of approximately 1 ms. Importantly, the magnitude of the association rate constant derived from the excess 2AP experiment is consistent with that from the excess RNA experiment (data not shown).

RNA−Ligand Complex Lifetime. Given the important role of the ligand−RNA complex lifetime (the time required for e^{-1} of a population to dissociate) in determining the characteristics of the *ribD* riboswitch (*11*), we sought to define the lifetime of the *pbuE* aptamer−ligand complex. To investigate the dissociation kinetics of 2AP, the association rate constant data were extrapolated to the *y*-intercept (Figure 3A), which yields the dissociation rate constant according to the relaxation equation:

$$\frac{1}{\tau} = k_{on}[2AP_{final} + RNA_{final}] + k_{off} \qquad (1)$$

Additionally, dilution−relaxation experiments (*26*, *27*) were performed in which the 2AP−RNA complex was diluted into fluorescently inert adenine to initiate a competition for the free RNA between adenine and the free 2AP that dissociated from the complex (Figure 4A, inset). The inverted reaction time constant at high adenine concentration yielded the dissociation rate constant of 2AP (Figure 4A). Both methods yielded similar 2AP k_{off} values of approximately 0.01 s^{-1} (Figure 4C), which is severalfold greater, or faster, than that for the FMN−*ribD* riboswitch complex. The lifetime of the 2AP−aptamer complex (calculated by inverting the dissociation rate constant) is 94, 44, and 18 s at 20, 25, and 30 °C, respectively.

Examination of eq 1 makes clear why knowledge of the dissociation rate constants is essential in order to discriminate between kinetic and equilibrium control of the riboswitch. According to the equation, at concentrations of 2AP that are small compared to K_D, the rate of approach to equilibrium ($1/\tau$) is dominated by k_{off} (assuming that the RNA concentration can be neglected). Furthermore, when the ligand (2AP) concentration is equal to K_D, which should lead to 50% occupancy of the RNA at equilibrium, it can be shown that

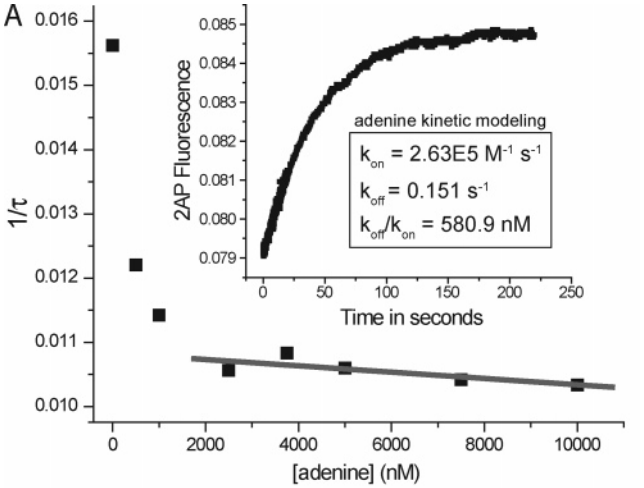

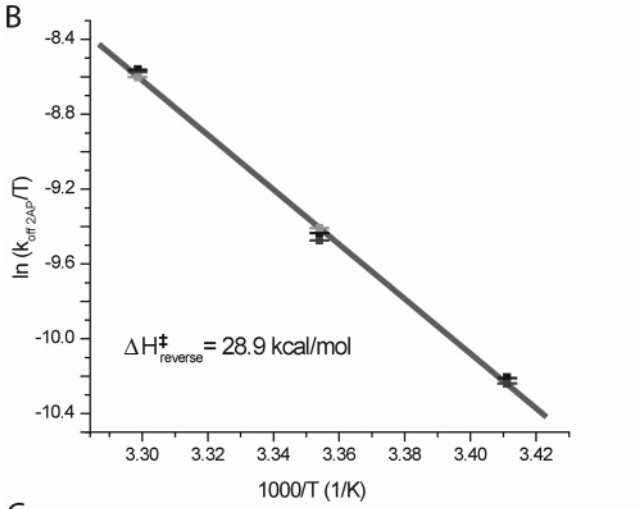

C

T (°C)	k_{off} (sec^{-1})	$\Delta G^{\ddagger}_{reverse}$	$\Delta G^{\ddagger}_{for} - \Delta G^{\ddagger}_{rev}$	ΔG°	K_D	k_{off}/k_{on}
20	10.61E-3	19.83	-8.5	-8.56	427	478
25	22.65E-3	19.70	-8.23	-8.35	764	910
30	56.83E-3	19.51	-8.2	-8.10	1480	1249

FIGURE 4: Dissociation rate constant of the 2AP−*pbuE* complex. (A) The inset is a sample set of data for the *pbuE*−2AP complex being diluted into adenine at 25 °C while monitoring 2AP fluorescence. The time constants from the dilution experiment, generated by a first-order exponential fit of the inset data, were inverted and plotted (black squares) against final adenine concentration. The *y*-axis value (highlighted by the linear fit) at high adenine concentration is taken as the 2AP dissociation rate constant. The adenine rate constants at 25 °C reported in the boxed inset were determined using the inset dilution data and kinetic modeling as described in Materials and Methods. (B) Eyring plot of the dissociation rate constants of 2AP generated in panel A. Each data point, a light gray, dark gray, or black cross, represents individual rate constant replicates. The slope of the plot, $\Delta H^{\ddagger}_{reverse}/R$, yields $\Delta H^{\ddagger}_{reverse} = 29$ kcal/mol. (C) Table of $\Delta G^{\ddagger}$ values calculated by Eyring theory. $\Delta G^{\ddagger}_{forward}$ and k_{on} were generated from Figure 3B, and ΔG° and K_D values of 2AP and 70 *pbuE*, in kilocalories per mole and nanomolar, were both generated from Figure 1.

90% of the equilibrium RNA binding level is reached by a time equal to about $1.15/k_{off}$. These considerations lead to the following simple kinetic test: if the time Δt_{RNAP} between completion of the aptamer by RNA polymerase and its progression to the termination decision point is comparable to or longer than $1/k_{off}$, the switch will approximate equilibrium control. However, if Δt_{RNAP} is much smaller than $1/k_{off}$, the switch is under kinetic control. Between these limits the control mode is mixed.

Analysis using an Eyring plot determined that the activation enthalpy for the 2AP dissociation rate constant was 28.9 kcal/mol (Figure 4B). Importantly, the difference between the activation free energy for the forward and reverse reactions corresponds to the free energy of the binding reaction as determined by the steady-state fluorometer experiments, further supporting a two-state binding model (Figure 4C). Additionally, from the association and dissociation rate studies it was determined that the kinetically derived K_D (k_{off}/k_{on}) was within 2-fold of the fluorescence-derived K_D of 2AP as well as within 2- and 3-fold of the K_D estimates based on in-line probing for adenine and 2AP, respectively. Given the k_{off} value of 2AP at 25 °C, the system would require in excess of 100 s (>2 times the dissociation lifetime) to approach equilibrium at low 2AP concentration. While this time scale could be accomplished with significant transcriptional pausing (*28*−*30*) within the expression platform domain, the 2AP−aptamer interaction would more likely be governed kinetically during transcription.

Contribution of Binding Kinetics to Ligand Discrimination. The fluorescence change of 2AP upon dissociation allowed an indirect measurement of the association and dissociation rate constants of adenine by kinetic competition experiments and subsequent modeling. Given an individual experiment where the k_{on} and k_{off} values for 2AP and the initial values of free adenine, 2AP, RNA, and RNA−2AP complex were known, the data were fit by kinetic simulation for adenine−RNA rate constants. The process was repeated at a range of adenine concentrations to ensure that the minimal two-state reaction model was valid. The rate constants determined at each concentration of adenine fell within 3-fold of each other and were averaged and reported (Figure 4A, boxed inset). The association and dissociation rate constants for adenine were each approximately 10-fold higher than the values for the interaction between 2AP and 70 *pbuE*. Hence, adenine and 2AP have similar kinetic K_D values, supporting the aforementioned equilibrium gel- and fluorescence-based K_D values as well as remaining consistent with a two-state binding model. From the dissociation rate constant data, the adenine−aptamer complex requires only about 15 s (>2 times the dissociation time constant) to approach equilibrium at 25 °C and low concentration, compared to ~100 s for 2AP. Given these values, the riboswitch could reasonably have either or both thermodynamic and kinetic character, depending upon the time scale of transcription.

Due to the high affinity the aptamer displayed for DAP (*20*), we endeavored to improve our confidence that the natural ligand of the *pbuE* riboswitch was adenine. If this genetic system operates at equilibrium, then even small amounts of DAP would inadvertently trigger the riboswitch. Likewise, if the association rate constant and the lifetime of the DAP−aptamer complex were both sufficiently large, then a kinetically governed riboswitch would sense cellular DAP over adenine. To address these issues, a kinetic competition assay was performed to determine the concentration of DAP required to compete equally with 2AP for the 70 *pbuE* RNA (Figure 5A). The reduction in the magnitude of the initial signal drop as the DAP concentration increases is indicative of similar DAP and 2AP association rate constants. Yet after the initial 2AP binding event, DAP clearly dominates the

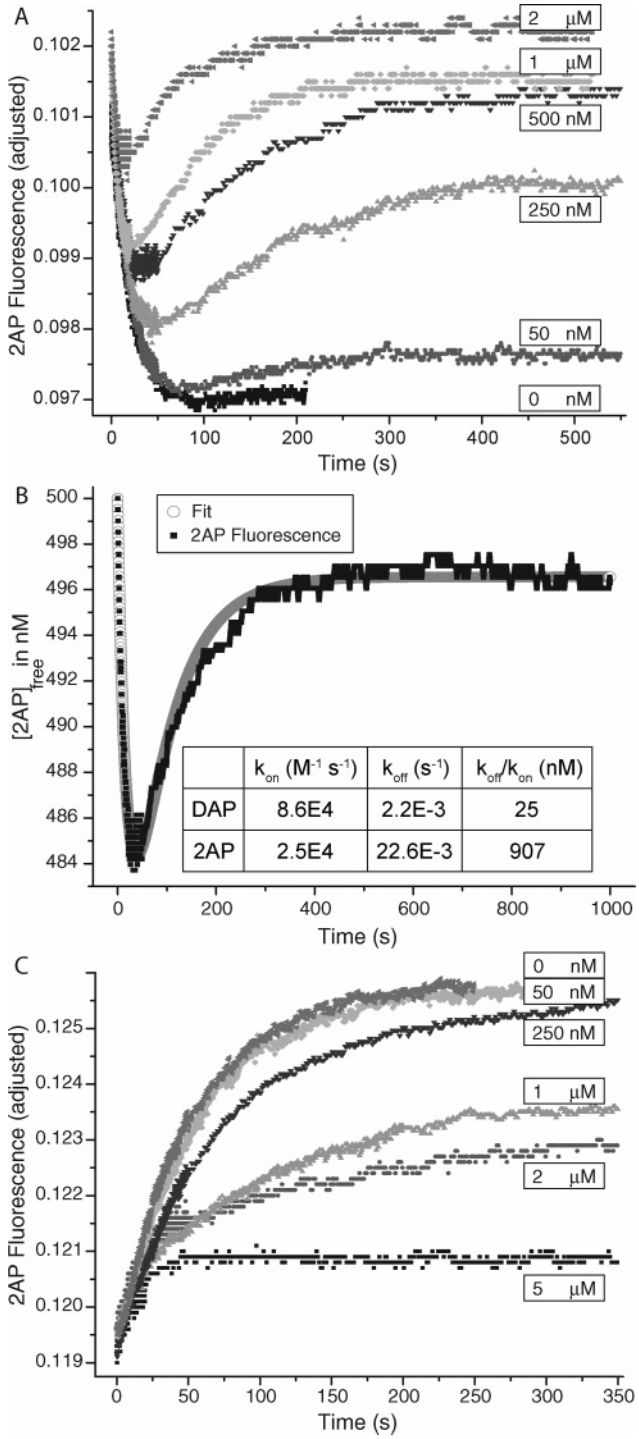

	k_{on} (M^{-1} s^{-1})	k_{off} (s^{-1})	k_{off}/k_{on} (nM)
DAP	8.6E4	2.2E-3	25
2AP	2.5E4	22.6E-3	907

FIGURE 5: DAP association and dissociation rate constants. (A) Diluted 100 nM (final) 70 *pbuE* RNA into a mixture of 500 nM 2AP and increasing total concentrations of DAP (legend) while monitoring 2AP fluorescence at 25 °C. (B) The 500 nM DAP data set from panel A fit by kinetic modeling described in the Materials and Methods section. The inset is a table of rate constant values generated from modeling. The kinetic values of 2AP binding were taken from Figures 3B and 4C. (C) A solution of 100 nM RNA and 500 nM 2AP (final) diluted into increasing DAP (final) monitoring the quenching of 2AP. The final DAP concentrations are as noted for each data set.

competition by binding the RNA and forcing the 2AP to remain unbound. The system was modeled and the data fit for values of k_{onDAP} and k_{offDAP} (Figure 5B and inset). Despite the similar association rate constants, the lifetime of the DAP−RNA complex is much longer than for 2AP, giving rise to the 40-fold lower kinetically determined K_D for DAP.

Additionally, a relaxation experiment was performed by diluting the RNA−2AP complex into increasing concentrations of DAP (Figure 5C). The results are consistent with the kinetic competition experiment in that when the concentration of free DAP equals 50 nM, formation of the 2AP−RNA complex is cut approximately in half as a result of DAP out-competing 2AP for the aptamer. In the presence of 100 nM RNA and 50 nM total DAP, we estimate that the free DAP concentration at equilibrium is 10−15 nM, or about 40-fold lower than the 2AP concentration, consistent with the ratio of kinetically determined K_D values. The relaxation experiment also provides evidence that the different ligands do not accelerate the dissociation of a rival ligand from the aptamer.

Definition of Kinetic and Thermodynamic Control Regimes. Since the rate constants for each ligand were determined, a simple kinetic simulation was performed to give insight into the kinetic and thermodynamic character of the riboswitch at 25 °C. A two-state binding model was used to simulate the kinetics, yielding the fraction of RNA bound over time given an initial concentration of 1 nM free 70 *pbuE* and discrete initial concentrations of ligand. We assume that in vivo changes in the fraction of full-length RNA induced by the ligand are proportional to changes in the fraction of RNA bound (*y*-axis of Figure 6). The rapid increase in the fraction bound in the early time points corresponds to a kinetically driven system, while the plateau in the curve is consistent with the reaction having reached equilibrium (Figure 6A). Pure kinetic control refers to the limit in which the relaxation time for equilibration of the adenine−aptamer complex is long compared to the time interval Δt_{RNAP} that begins when enough sequence has exited the polymerase to form the aptamer and ends when the transcription termination decision point has been reached. In this case the regulatory concentration B_{50} (B_{50} is the midpoint in the response curve of adenine binding versus concentration) depends primarily on the adenine association rate constant. In the thermodynamic limit, the relaxation time is short compared to the transcriptional time scale Δt_{RNAP} (which includes possible transcriptional pausing), and B_{50} is sensitive to the equilibrium dissociation constant, K_D. Between these two regimes there is a transition that is comprised of a mixture of each character; the lifetime of this intervening region, termed "mixed" and defined as approximately from 75% to 95% of the fraction of RNA bound, is highly dependent upon the concentration of ligand (Figure 6B). To describe the behavior of the system, a comparison must be made between the lifetime of the first binding phase (from 0% to 75% bound) and Δt_{RNAP}. Should this "binding-competent window" be less than the time to complete ~75% of the equilibrium binding level, the switch would be kinetically driven. For example, the lifetime of the kinetic regime of the system with 1 μM adenine is on the order of 5 s, but the lifetime drops to under 1 s if 10 μM adenine is present (Figure 6B and inset). The aptamer reaches equilibrium with 2AP and DAP on slower time scales, corresponding to their smaller association rate constants.

To investigate the results of a kinetic competition between adenine and DAP, a simulation was performed in which 10 μM adenine and various concentrations of DAP compete

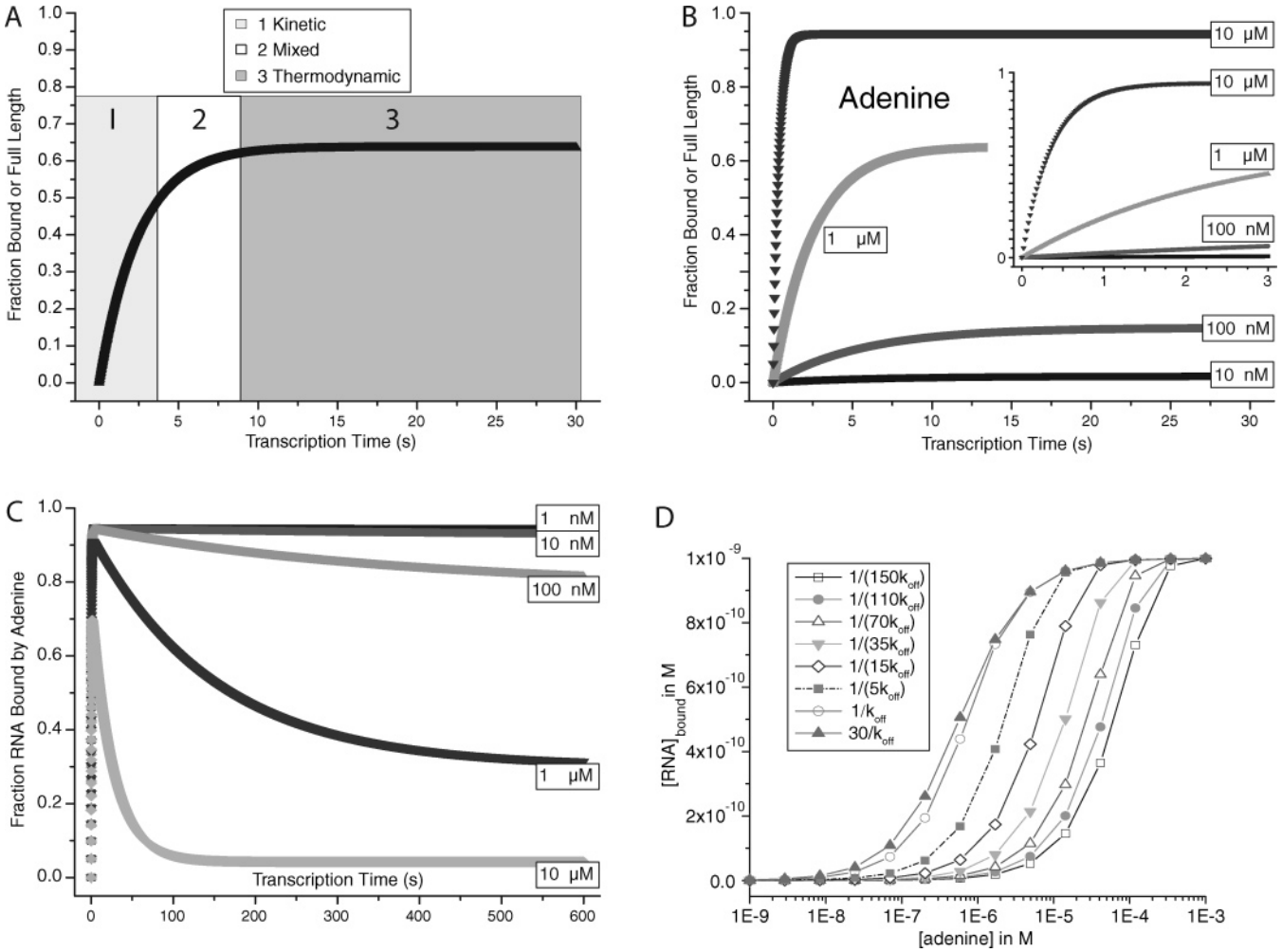

FIGURE 6: Kinetic simulation of binding and genetic decision using kinetic constants determined at 25 °C. (A) A sample set of data. The *y*-axis represents the fraction of bound aptamer and the fraction of full-length transcript. The purely kinetic, mixed, and purely thermodynamic zones of character are marked by the light gray (1), white (2), and dark gray (3) background. The partition between zones was set by defining the mixed region from approximately 75−95% of the fraction bound; time domains below and above this zone are designated kinetic and thermodynamic, respectively. (B) Simulated data for the interaction between 70 *pbuE* RNA and adenine over time. Lines are labeled with the initial adenine concentration of 10 nM, 100 nM, 1 μM, and 10 μM, respectively. The inset is a magnified view of the first tenth of the time course (3 s). (C) Kinetic simulation of the competition between adenine (10 μM initial free concentration) and various initial free concentrations of DAP (as indicated) for binding 70 *pbuE* RNA (1 nM initial free concentration). Note that adenine has the advantage at early times because of its larger k_{on} but that DAP (at 1 or 10 μM) dominates binding at equilibrium because of its smaller K_D. (D) Simulated dependence of the extent of adenine binding to the riboswitch at 25 °C using the kinetic parameters reported in Figure 4. A 1 nM concentration of RNA is assumed. The different curves correspond to different values of Δt_{RNAP}, expressed as factors of $1/k_{off}$, where k_{off} is the dissociation rate constant. For the conditions of Figure 4, $1/k_{off}$ is about 6.5 s. The maximum value of Δt_{RNAP} assumed in the simulation is $30/k_{off}$, or about 200 s. Under these conditions binding is at equilibrium, and B_{50} is equal to the K_D. Deviations from equilibrium, particularly at low adenine concentrations, are apparent when $\Delta t_{RNAP} = 1/k_{off}$. As Δt_{RNAP} becomes progressively smaller, B_{50} moves to higher adenine concentrations. A noteworthy feature of the curves is their asymmetry and the abrupt transition to saturation binding when the system is under kinetic control.

directly for 1 nM 70 *pbuE* RNA (Figure 6C). DAP does not begin to hinder the initial binding of adenine until reaching the micromolar level. Even at 10 μM DAP, about 70% of the aptamer population initially binds adenine, which is a consequence of the ~3-fold advantage enjoyed by adenine in the association rate constant. However, the fraction of bound adenine decreases rapidly with time, which reflects the fast dissociation of adenine and tighter equilibrium binding of DAP with the aptamer. The simulations begin to define the kinetic and thermodynamic character of the riboswitch and give insight into the probable biological target ligand: adenine. Yet the expression platform will make the genetic decision to transcribe the full-length message regardless of which ligand is bound to the aptamer at the time of the decision; as long as any ligand is bound, the genetic decision will result in the full-length message. Further, it is evident that the faster the time scale of transcription, the more likely adenine will be the ligand of choice for the aptamer (Figure 6C).

The simulations were also used to generate mock data of the kind that can be generally determined experimentally for riboswitches, showing the concentration dependence of the switch properties. Using the experimental parameters determined for adenine (Figure 4), we assumed a range of values for Δt_{RNAP} varying from $30/k_{off}$ to $1/150k_{off}$. The longest of these transcriptional delay times, $30/k_{off}$, allows enough time for equilibrium to be established. As shown by Figure 6D, for the curve with $\Delta t_{RNAP} = 1/k_{off}$ deviations between the equilibrium curve and the simulated value of adenine binding are significant at ligand concentrations below K_D. These

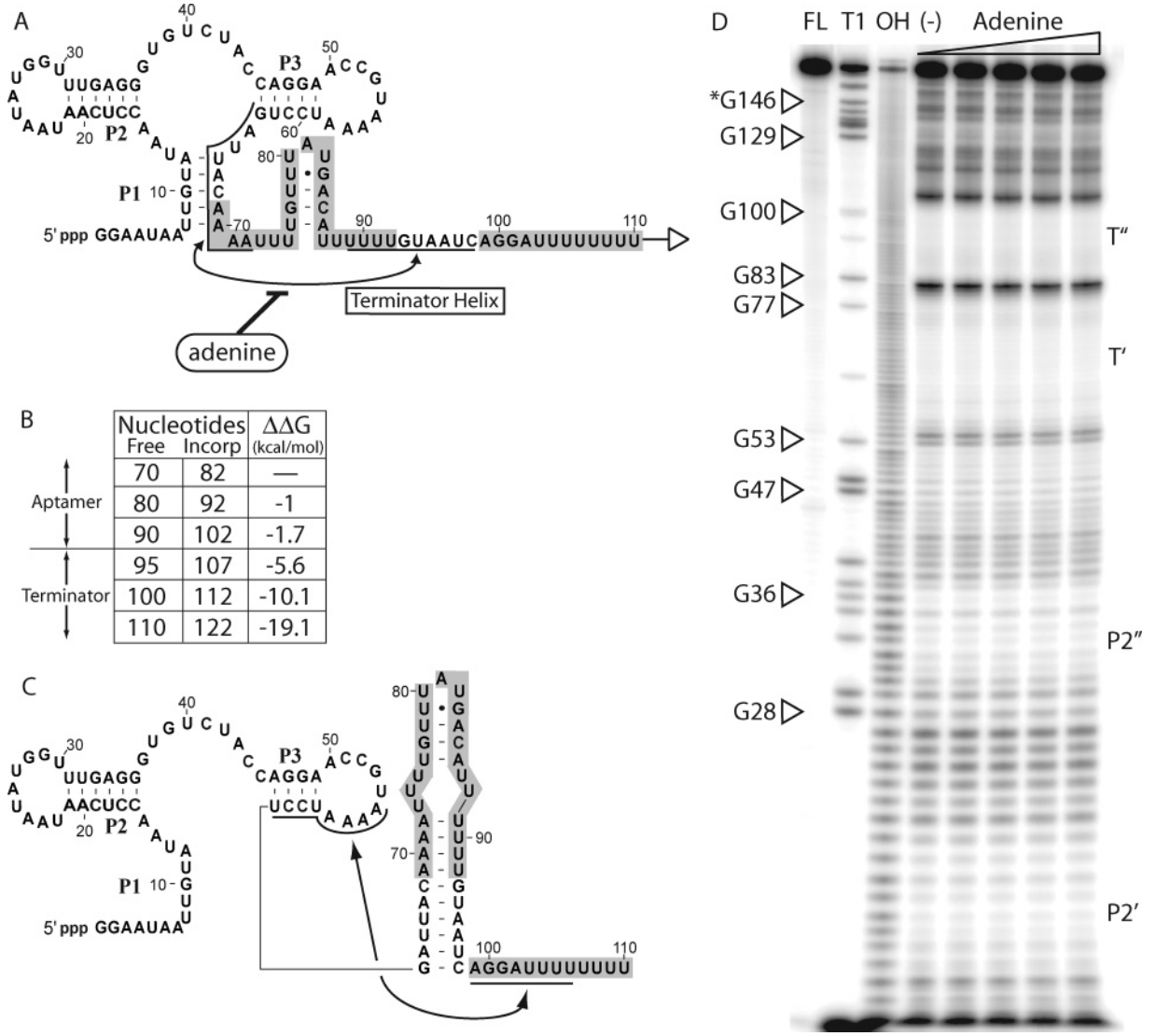

FIGURE 7: Adenine riboswitch structural model. (A) Secondary structural model generated from the purine riboswitch phylogeny, representing the bound aptamer state yielding a full-length transcript. The gray boxes represent a polymerase toeprint of 12 nucleotides at putative transcriptional pause sites. The arrowed lines highlight the bases that pair to form the termination helix while the polymerase is incorporating a nucleotide at approximately position 110. Adenine inhibits the formation of the terminator helix and results in the formation of the full-length transcript. (B) Table of $\Delta\Delta G°$ values generated computationally from the program RNAstructure. All $\Delta\Delta G°$ values are based on 70 *pbuE*. The "incorp" column represents the approximate nucleotide being incorporated by the polymerase at that point in the transcription. (C) The structural model represents the ligand-free termination structure assuming the polymerase obscures 12 bases while incorporating the last nucleotide of the terminated transcript. The arrowed lines represent the RNA forming the full termination helix, presumably to favor complete dissociation of the polymerase. (D) In-line probing assay on the full-length RNA (175 pbuE). From left to right the lanes denote a full-length RNA, partial RNA digest with RNase T1, partial RNA digest with alkali, and RNA incubated at 25 °C for 40 h in 0, 100 nM, 1 μM, 10 μM, and 100 μM adenine. P2′ indicates nucleotides 16−21. P2″ indicates nucleotides 31−36. T′ indicates nucleotides 55−79. T″ indicates nucleotides 83−106.

conditions constitute a mixed mode of control. At higher concentrations, the resulting faster relaxation brings the kinetic simulation and the equilibrium value of binding into close correspondence. However, as Δt_{RNAP} becomes even smaller, kinetic control takes over, so that B_{50} values become progressively larger. It is also noteworthy that that the concentration response curves become more abrupt at the high concentration limit in the kinetic control regime. For example, when $\Delta t_{RNAP} = 30/k_{off}$ (the equilibrium case), a 190-fold decrease of ligand concentration is required to reduce the switch occupancy from 99% to 50%. For $\Delta t_{RNAP} = 1/150k_{off}$ (kinetic control), the ligand concentration has to decrease by only 10-fold to achieve the same occupancy alteration. This effect could be mistakenly construed as evidence for cooperative binding.

Ligand Binding Competency during Transcription. During active transcription of a riboswitch, a ligand binding-competent sequence exists in a temporal window Δt_{RNAP}, prior to which the nascent aptamer transcript has not cleared the polymerase and after which the genetic decision has been made. The ligand is not able to bind *pbuE* until the aptamer is formed, which occurs when approximately 80 nucleotides have been incorporated (Figure 7A), assuming a polymerase toeprint of 10−12 nucleotides (gray boxes in Figure 7) (*31*, *32*). The binding-competent window, defined approximately by progressive incorporation of nucleotides 80−110 into the transcript (from the point at which the aptamer can form until the point at which the terminator will form), would pass in 2 s if the polymerase incorporated approximately 15 bases each second (*33*, *34*). The measured association rate constant

for 70 *pbuE* and adenine (2.6×10^5 M^{-1} s^{-1} at 25 °C) requires 2 μM free adenine to significantly bind the aptamer within this putative 2 s temporal window of opportunity. The simulated ligand response curves in Figure 6D show how the system responds to changes in the value of Δt_{RNAP}, which cause the control mechanism to switch between kinetic and equilibrium modes.

We also sought to verify that the ligand binding-competent window ends when the terminator helix is formed. From in-line assay probing experiments, it is observed that even at 100 μM adenine the equilibrium conformation of the full-length mRNA leader (175 *pbuE*) is fixed in the binding-incompetent terminator structure (Figure 7C). These data agree with the structural predictions for this RNA; the decision must happen prior to the formation of the full terminator helix, defined by nucleotides 63−72 and 73−79 base pairing with nucleotides 83−86 and 89−98, respectively.

RNA Structural Energetics during Transcription. Another potentially rate-limiting process that must occur during Δt_{RNAP} if termination is to be the outcome is an RNA conformational switch to form the terminator helix in the absence of adenine binding. We postulate, given the energetics of the RNA folds predicted by the program RNAstructure (*22*) and assuming a 12-nucleotide toeprint of the RNAP on the nascent transcript, that the aptamer conformation will dominate the *pbuE* RNA until the RNAP incorporates about nucleotide 105 (Figure 7B). From that point onward, there is enough primary sequence to shift the equilibrium significantly away from the aptamer fold and toward the binding-incompetent terminator structure. Given the sizable rearrangement of secondary structure required for the fold to shift from aptamer to terminator, important questions remain: is the folding reaction in equilibrium and how fast does this structural transition occur? Whether or not the folding reaction reaches equilibrium depends on its rate, which depends on the folding reaction activation energy barrier. The energy difference between the fully folded 90 *pbuE* RNA favoring the aptamer structure and the same RNA in which nucleotides 66−80 (the bases used to nucleate the terminator helix) are kept single stranded can be used as a first-order estimation of the transition state barrier magnitude. The resulting free energy difference between the aptamer ground state and the semistructured intermediate is predicted to be only 1.2 kcal/mol at 37 °C. Given that thermal noise per degree of freedom at room temperature is half this value (universal gas constant, *R*, multiplied by temperature), the estimated activation barrier appears to be small enough to allow an easy kinetic transition from the aptamer fold to the terminator structure. Further, even in the absence of adenine during transcription, the sequence comprising the aptamer fold appears first, so this structure must be overcome in order for the default termination structure to arise during each individual transcription event.

Other biological RNAs exhibit facile switching back and forth between two stable states in a manner that seems to bypass or cut through the activation energy barrier associated with the melting out of one state in order to form the other. For example, a spliced leader RNA in *Leptomonas collosoma* exhibits two conformational states (*35*). The rapid interconversion (<1 s) between the two structures implies a putative short-lived transition state structure that bridges the two observable states and precludes the need to overcome the activation energy barrier, which would be expected to be approximately equal to the bond dissociation energy and would relegate the interconversion to a much slower time scale (*36*). From these studies it is likely that the interconversion between the aptamer and the terminator conformations of *pbuE* is possible at a rate faster than the rate of transcription, despite the required secondary structural changes.

The behavior of the *pbuE* riboswitch may be further studied by identifying controlling elements within the primary sequence of the RNA. There exist two series of U residues (Figure 7A, nucleotides 73−80 and 87−92) after the aptamer but before the terminator-associated series of U bases that fit the transcriptional pause site profile set in the *ribD* RNA system (*11*). Likewise, the FMN-dependent riboswitch in the *ribD* RNA had two pauses that assisted the riboswitch function by providing the RNA additional time to fold correctly and bind the ligand prior to the polymerase making the antiterminator strand available. Without an estimation of the lifetime of these putative transcriptional pause sites, no conclusions can be drawn about their impact upon the thermodynamic and kinetic character of this riboswitch. So it is possible that any pausing is functional and provides the time required for thermodynamics to govern the switch behavior, or the pauses, whose lifetimes are dependent upon the concentration of nucleotides and the presence of transcription cofactors such as NusA (*37*), act as a further biological sensor of these factors. For example, if the nucleotide concentration drops, thus lengthening the lifetime of the pause sites, the concentration of adenine required to bind the aptamer and produce full-length transcripts will drop down toward the K_D value. Thus, it is transcription of the expression platform domain that ultimately defines the kinetic or thermodynamic character of a riboswitch system. Further, the expression platform domain adds additional control points by which the organism may further refine homeostasis by genetic changes, including altering the lifetime and frequency of transcriptional pause sites, modulating the stability and formation kinetics of the binding-incompetent RNA structure, and modulating terminator stem stability.

In summary, the *pbuE* riboswitch, an ON switch, is capable of binding the three ligands studied in this report. However, the likely biological target is adenine due to the placement of the *pbuE* gene product within the adenine metabolic pathway (*13*, *14*, *20*) and the kinetic parameters of binding adenine to the *pbuE* aptamer. It is believed, based upon kinetic simulations using the measured values of the association and dissociation rate constants of adenine and the aptamer RNA, that this riboswitch could function as a kinetically or a thermodynamically controlled genetic switch depending upon the transcription time scale and the transcriptional components impacting that time scale.

Riboswitches represent an important strategy in genetic control that might be a fossil of the RNA world, yet their simplicity and energetically conservative nature help to provide organisms from all three kingdoms of life the tools necessary to function in biology today. While more research is required to completely dissect the intricate mechanistic details of this and other riboswitches in the context of active

transcription, this work further establishes the general principles by which these important RNAs function.

REFERENCES

1. Winkler, W. C., and Breaker, R. R. (2003) Genetic control by metabolite-binding riboswitches, *ChemBioChem 4*, 1024−1032.
2. Mandal, M., and Breaker, R. R. (2004) Gene regulation by riboswitches, *Nat. Rev. Mol. Cell Biol. 5*, 451−463.
3. Mandal, M., Lee, M., Barrick, J. E., Weinberg, Z., Emilsson, G. M., Ruzzo, W. L., and Breaker, R. R. (2004) A glycine-dependent riboswitch that uses cooperative binding to control gene expression, *Science 306*, 275−279.
4. Nudler, E., and Mironov, A. S. (2004) The riboswitch control of bacterial metabolism, *Trends Biochem. Sci. 29*, 11−17.
5. Vitreschak, A. G., Rodionov, D. A., Mironov, A. A., and Gelfand, M. S. (2004) Riboswitches: the oldest mechanism for the regulation of gene expression?, *Trends Genet. 20*, 44−50.
6. Winkler, W. C., Nahvi, A., Roth, A., Collins, J. A., and Breaker, R. R. (2004) Control of gene expression by a natural metabolite-responsive ribozyme, *Nature 428*, 281−286.
7. Winkler, W. C., Nahvi, A., and Breaker, R. R. (2002) Thiamine derivatives bind messenger RNAs directly to regulate bacterial gene expression, *Nature 419*, 952−956.
8. Winkler, W. C., Cohen-Chalamish, S., and Breaker, R. R. (2002) An mRNA structure that controls gene expression by binding FMN, *Proc. Natl. Acad. Sci. U.S.A. 99*, 15908−15913.
9. Kubodera, T., Watanabe, M., Yoshiuchi, K., Yamashita, N., Nishimura, A., Nakai, S., Gomi, K., and Hanamoto, H. (2003) Thiamine-regulated gene expression of *Aspergillus oryzae* thiA requires splicing of the intron containing a riboswitch-like domain in the 5′-UTR, *FEBS Lett. 555*, 516−520.
10. Sudarsan, N., Barrick, J. E., and Breaker, R. R. (2003) Metabolite-binding RNA domains are present in the genes of eukaryotes, *RNA 9*, 644−647.
11. Wickiser, J. K., Winkler, W. C., Breaker, R. R., and Crothers, D. M. (2005) The speed of RNA transcription and ligand binding kinetics operate an FMN binding riboswitch, *Mol. Cell 18*, 49−60.
12. Sudarsan, N., Wickiser, J. K., Nakamura, S., Ebert, M. S., and Breaker, R. R. (2003) An mRNA structure in bacteria that controls gene expression by binding lysine, *Genes Dev. 17*, 2688−2697.
13. Johansen, L. E., Nygaard, P., Lassen, C., Agerso, Y., and Saxild, H. H. (2003) Definition of a second *Bacillus subtilis* pur regulon comprising the pur and xpt-pbuX operons plus pbuG, nupG (yxjA), and pbuE (ydhL), *J. Bacteriol. 185*, 5200−5209.
14. Nygaard, P., and Saxild, H. H. (2005) The purine efflux pump PbuE in *Bacillus subtilis* modulates expression of the PurR and G-Box (XptR) regulons by adjusting the purine base pool size, *J. Bacteriol. 187*, 791−794.
15. Mandal, M., Boese, B., Barrick, J. E., Winkler, W. C., and Breaker, R. R. (2003) Riboswitches control fundamental biochemical pathways in *Bacillus subtilis* and other bacteria, *Cell 113*, 577−586.
16. Serganov, A., Yuan, Y. R., Pikovskaya, O., Polonskaia, A., Malinina, L., Phan, A. T., Hobartner, C., Micura, R., Breaker, R. R., and Patel, D. J. (2004) Structural basis for discriminative regulation of gene expression by adenine- and guanine-sensing mRNAs, *Chem. Biol. 11*, 1729−1741.
17. Batey, R. T., Gilbert, S. D., and Montange, R. K. (2004) Structure of a natural guanine-responsive riboswitch complexed with the metabolite hypoxanthine, *Nature 432*, 411−415.
18. Lescoute, A., and Westhof, E. (2005) Riboswitch structures: purine ligands replace tertiary contacts, *Chem. Biol. 12*, 10−13.
19. Noeske, J., Richter, C., Grundl, M. A., Nasiri, H. R., Schwalbe, H., and Wohnert, J. (2005) An intermolecular base triple as the basis of ligand specificity and affinity in the guanine- and adenine-sensing riboswitch RNAs, *Proc. Natl. Acad. Sci. U.S.A. 102*, 1372−1377.
20. Mandal, M., and Breaker, R. R. (2004) Adenine riboswitches and gene activation by disruption of a transcription terminator, *Nat. Struct. Mol. Biol. 11*, 29−35.
21. Eisenberg, D. S., and Crothers, D. M. (1979) *Physical chemistry: with applications to the life sciences*, Benjamin/Cummings, Menlo Park, CA.
22. Mathews, D. H., Disney, M. D., Childs, J. L., Schroeder, S. J., Zuker, M., and Turner, D. H. (2004) Incorporating chemical modification constraints into a dynamic programming algorithm for prediction of RNA secondary structure, *Proc. Natl. Acad. Sci. U.S.A. 101*, 7287−7292.
23. Soukup, G. A., and Breaker, R. R. (1999) Relationship between internucleotide linkage geometry and the stability of RNA, *RNA 5*, 1308−1325.
24. Ward, D. C., Reich, E., and Stryer, L. (1969) Fluorescence studies of nucleotides and polynucleotides. I. Formycin 2-aminopurine riboside 2,6-diaminopurine riboside and their derivatives, *J. Biol. Chem. 244*, 1228−1237.
25. Chaires, J. B., Dattagupta, N., and Crothers, D. M. (1985) Kinetics of the daunomycin−DNA interaction, *Biochemistry 24*, 260−267.
26. Li, H. J., and Crothers, D. M. (1969) Relaxation studies of the proflavine-DNA complex: the kinetics of an intercalation reaction, *J. Mol. Biol. 39*, 461−477.
27. Zeman, S. M., Depew, K. M., Danishefsky, S. J., and Crothers, D. M. (1998) Simultaneous determination of helical unwinding angles and intrinsic association constants in ligand-DNA complexes: The interaction between DNA and calichearubicin B, *Proc. Natl. Acad. Sci. U.S.A. 95*, 4327−4332.
28. Winkler, M. E., and Yanofsky, C. (1981) Pausing of RNA polymerase during in vitro transcription of the tryptophan operon leader region, *Biochemistry 20*, 3738−3744.
29. Shundrovsky, A., Santangelo, T. J., Roberts, J. W., and Wang, M. D. (2004) Single molecule studies of sequence-dependent transcription pausing, *Biophys. J. 87*, 3945−3953.
30. Pan, T., Artsimovitch, I., Fang, X. W., Landick, R., and Sosnick, T. R. (1999) Folding of a large ribozyme during transcription and the effect of the elongation factor NusA, *Proc. Natl. Acad. Sci. U.S.A. 96*, 9545−9550.
31. Monforte, J. A., Kahn, J. D., and Hearst, J. E. (1990) RNA folding during transcription by *Escherichia coli* RNA polymerase analyzed by RNA self-cleavage, *Biochemistry 29*, 7882−7890.
32. Komissarova, N., and Kashlev, M. (1998) Functional topography of nascent RNA in elongation intermediates of RNA polymerase, *Proc. Natl. Acad. Sci. U.S.A. 95*, 14699−14704.
33. Adelman, K., La Porta, A., Santangelo, T. J., Lis, J. T., Roberts, J. W., and Wang, M. D. (2002) Single molecule analysis of RNA polymerase elongation reveals uniform kinetic behavior, *Proc. Natl. Acad. Sci. U.S.A. 99*, 13538−13543.
34. Tolic-Norrelykke, S. F., Engh, A. M., Landick, R., and Gelles, J. (2004) Diversity in the rates of transcript elongation by single RNA polymerase molecules, *J. Biol. Chem. 279*, 3292−3299.
35. Lecuyer, K. A., and Crothers, D. M. (1993) The *Leptomonas collosoma* spliced leader RNA can switch between 2 alternate structural forms, *Biochemistry 32*, 5301−5311.
36. LeCuyer, K. A., and Crothers, D. M. (1994) Kinetics of an RNA conformational switch, *Proc. Natl. Acad. Sci. U.S.A. 91*, 3373−3377.
37. Yakhnin, A. V., and Babitzke, P. (2002) NusA-stimulated RNA polymerase pausing and termination participates in the *Bacillus subtilis* trp operon attenuation mechanism in vitro, *Proc. Natl. Acad. Sci. U.S.A. 99*, 11067−72.

BI051008U